ACS PHYSICAL CHEMISTRY Au
AN OPEN ACCESS JOURNAL OF THE AMERICAN CHEMICAL SOCIETY

pubs.acs.org/physchemau

Article

Analysis of the Passage Times for Unfolding/Folding of the Adenine Riboswitch Aptamer

Shivangi Sharma,[†] Vishal Singh,[†] and Parbati Biswas*

Cite This: *ACS Phys. Chem Au* 2022, 2, 353−363

Read Online

ACCESS | Metrics & More | Article Recommendations

ABSTRACT: The conformational transitions of the adenosine deaminase A-riboswitch aptamer both with and without ligand binding are investigated within the tenets of the generalized Langevin equation in a complex viscoelastic cellular environment. Steered molecular dynamics (SMD) simulations are performed to evaluate and compare the results of the first passage times (FPTs) with those obtained from the theory for the unfold and fold transitions of the aptamer. The results of the distribution of Kramers's FPT reveal that the unfold-fold transitions are faster and hence more probable as compared to the fold-unfold transitions of the riboswitch aptamer for both ligand-bound and -unbound states. The transition path time is lower than Kramers's FPT for the riboswitch aptamer as the transition path times for the unfold-fold transition of both without and with ligand binding are insensitive to the details of the exact mechanism of the transition events. However, Kramers's FPTs show varied distributions which correspond to different transition pathways, unlike the transition path times. The mean FPT increases with an increase in the complexity of the cellular environment. The results of Kramers's FPT, transition path time distribution, and mean FPT obtained from our calculations qualitatively match with those obtained from the SMD simulations. Analytically derived values of the mean transition path time show good quantitative agreement with those estimated from the single-molecule force spectroscopy experiments for higher barrier heights.

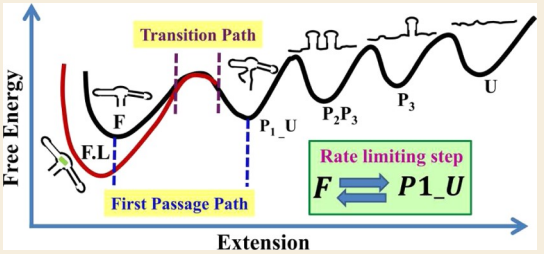

KEYWORDS: *generalized Langevin equation, probability distribution function, steered molecular dynamics simulation, first passage time, fold-unfold transition, transition path time, survival probability*

1. INTRODUCTION

Purine (adenine or guanine) riboswitches comprise the gene regulatory elements in mRNA that contain a ligand-binding aptamer domain specific for binding the ligand adenine/guanine.[1,2] The adenosine deaminase (*add*) A-riboswitch is a purine riboswitch composed of an assembly of three helical stems or hairpins (P1, P2, and P3) with two interacting loops (L2 and L3) that resembles the geometry of that of a tuning fork[3−5] (refer to Figure 1). Reversible switching between two conformations by binding to a target ligand or other cellular metabolites affects the aptamer-folding pattern that regulates gene expression, protection of genomes, molecular recognition, and catalysis.[6,7] Single-molecule force spectroscopy (SMFS) experiments investigate the multistep hierarchical unfolding/folding pathways of the riboswitch aptamer.[3,8,9] Typically, these experiments measure the extension of the molecule while it folds and unfolds in the presence or absence of the ligand (adenine) under the applied force of varying magnitudes through optical/laser tweezers[10,11] or an atomic force microscope.[12,13] The results obtained from these experiments established that ligand binding stabilizes the aptamer domain, and the conformational transition in the free energy landscape may be correlated to different degrees of secondary and tertiary interactions along the folding trajectory.[14,15]

The transitions of any biomolecule between different possible conformations have been analyzed within the framework of barrier crossing dynamics.[16−19] The conformational transition of the *add* A-riboswitch between two states in a one-dimensional (1D) free energy landscape may be classified into two sets of trajectories:[20,21] (a) that starts from one state located at a potential well and crosses the free energy barrier to reach the other state without revisiting the initial state (i.e., direct transit or transition path) and (b) that starts from one state corresponding to a potential energy minimum and reaches the other state at a different potential energy minimum across the free energy barrier with multiple recrossings (i.e., first passage path). The times required for the trajectories (a) and (b) are termed as transition path time

Received: December 27, 2021
Revised: April 5, 2022
Accepted: April 5, 2022
Published: April 26, 2022

ACS Publications
© 2022 The Authors. Published by American Chemical Society

https://doi.org/10.1021/acsphyschemau.1c00056
ACS Phys. Chem Au 2022, 2, 353−363

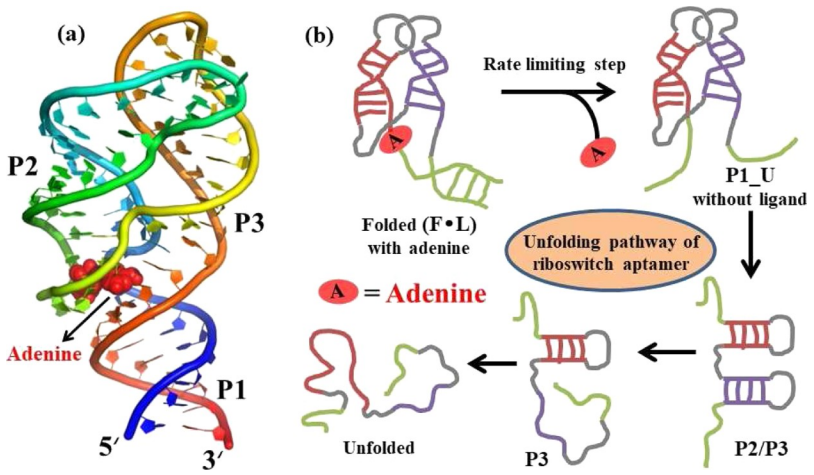

Figure 1. (a) Tertiary structure of the *add* A-riboswitch aptamer (PDB ID: 1Y26). (b) Pathway of unfolding of the aptamer, where F·L denotes the riboswitch aptamer with the adenine (A)-bound ligand.

(TPT) and first passage time (FPT) or Kramer's FPT, respectively. Both transitions and the FPT may be mathematically described by the Fokker–Planck equation (FPE) with suitable boundary conditions.[21,22] The transition path is defined as the fragment of the molecular trajectory where the molecule just crosses the potential energy barrier during the transition from one conformation to the other without revisiting its initial conformation.[18,23] The FPT includes the total time required by the riboswitch to dwell in between the two preferred conformations located at the two potential minima along with the TPT. Unlike FPT, TPT only includes the time required to just cross the potential barrier without revisits. Both the first passage path and transition path contain all microscopic information to understand barrier crossing dynamics of proteins and nucleic acids.

This work presents an analysis of the stochastic dynamics of the conformational transitions of the *add* A-riboswitch aptamer both with and without ligand binding in viscoelastic complex cellular environments within the framework of generalized Langevin equation (GLE). Theoretical results provide a quantitative estimate of the typical transit times for such conformational transitions along with the exact shape of such distributions, which are difficult to determine experimentally. A qualitative comparison of the analytical results of the transition path and Kramer's FPT with those obtained from the steered molecular dynamics (SMD) simulations (for TPT calculations from SMD, refer to ref 5) shows that the TPT for the ligand-induced unfold-fold transitions of the *add* A-riboswitch aptamer is insensitive to the mechanism of the transition process as compared to Kramers's FPT.[9] The FPT analysis also reveals that the unfold-fold transitions of the riboswitch aptamer are more probable and faster as compared to the fold-unfold ones. Survival probability follows a stretched Mittag-Leffler decay for the unfold and fold transitions, where the probability of the aptamer in the ligand-bound state shows a much slower decay as compared to that in the ligand-unbound state. The mean FPT (MFPT) and the mean TPT (MTPT) of the unfold-fold transitions of the riboswitch increase with the increase in the complexity of surroundings due to the "caging" effect. The distribution of the TPT,[5] Kramer's FPT, and the MFPT for both fold and unfold transitions of the riboswitch aptamer both with and without ligand binding obtained from theory is in good qualitative agreement with those of SMD simulations. The theoretical values of the MTPT estimated quantitatively agree with those obtained from the SMFS experiments[9] for higher barrier heights.

2. THEORY

SMFS experiments have established that the structural transitions of the riboswitch aptamer[24,25] both with and without ligand (adenine) binding follow a five-step folding pathway which may be modeled as a discrete assembly of multiple distinct two-state transition processes across a potential energy barrier between two wells in an asymmetric free energy landscape. The schematic diagrams of the unfolding pathway of the riboswitch aptamer F → P1_U → P2/P3 → P3 → U in the free energy landscape are schematically illustrated in Figure 1. Numerous tertiary contacts which are present at the three-way junction of the secondary structure of the riboswitch aptamer govern the active binding of adenine to the aptamer. The ligand binding stabilizes the riboswitch aptamer domain via the enhancement of secondary and/or tertiary contacts/interactions. Several experimental studies have established that ligand binding stabilizes the riboswitch structure, which implies reduced populations of other intermediate states in the entire folding pathway. Hence, the transitions to P2/P3 states are not prominent and thus are neglected. This suggests that ligand binding of the aptamer defines an unfold or refold transition from the fully folded state F to the unfolded P1_U state or vice versa (i.e., F → P1_U or P1_U → F), respectively, which is the rate-determining step in the aptamer folding.[24] The dynamics of the unfold and fold transitions of the riboswitch aptamer may be expressed in terms of a simple 1D diffusion model[5,22] where different transitions are determined by an appropriate reaction coordinate, x. This reaction coordinate is defined as the distance between the two termini or any two randomly selected base pairs of the nucleotides of the aptamer both with and without ligand binding. Experimentally, x denotes the extension of the riboswitch aptamer in response to an applied force of varying magnitudes.[3,24] Thus, the time evolution of the reaction coordinate, $x(t)$ for both unfold-fold and fold-unfold transitions with and without ligand binding in complex viscoelastic cellular environments, may be described within the tenets of the overdamped GLE, as[5,22,26,27]

https://doi.org/10.1021/acsphyschemau.1c00056
ACS Phys. Chem Au 2022, 2, 353−363

$$m\int_0^t \gamma(t-t')\dot{x}(t')\,dt' = -\frac{dU(x)}{dx} + \xi(t) \tag{1}$$

where $x(t)$ is the time-dependent extension of the riboswitch aptamer and $U(x)$ denotes the effective potential (or free energy). $\xi(t)$ indicates the long-time correlated thermal fluctuations imparted by the surrounding cellular medium with zero mean, $\langle\xi(t)\rangle = 0$. The noise term is related to the time-dependent frictional memory kernel $\gamma(t)$ through the fluctuation dissipation theorem.[26] The correlated thermal fluctuations may be modeled by $\gamma(t)$ that accounts for the non-Markovian dynamics[5,28,29] represented as

$$\langle\xi(t)\xi(0)\rangle = \frac{k_B T\eta_\beta t^{-\beta}}{\Gamma(1-\beta)} \tag{2}$$

where η_β represents the fractional friction coefficient that may be expressed as $\eta_\beta = \eta/\tau_c^{(1-\beta)}$, τ_c is the correlation time, and Γ denotes the gamma function. The scaling exponent, β, with $0 < \beta \leq 1$ determines the degree of the complexity/heterogeneity of the surrounding environment, where $\beta = 0$ depicts a completely heterogeneous (viscoelastic) environment and $\beta = 1$ corresponds to completely homogeneous (diffusive) surroundings.

SMFS experiments record the force extension curves of the fold and unfold trajectories of the *add* A-riboswitch aptamer both with and without ligand binding, where it folds and unfolds under controlled load applied by optical traps.[24] The free energy profiles determined from these experiments indicate that the two states (i.e., F and P1_U) are of unequal energy and hence the fold-unfold transition may be modeled as a conformational transition in an asymmetric bistable potential well. However, adenine binding (i.e., F·L) further stabilizes the folded state of the aptamer due to an increase in the tertiary and secondary interactions that stabilizes the fully folded state of the aptamer by an additional −8 kcal/mol as compared to the unbound one.[3]

This asymmetric double-well potential may be represented by a generalized expression defined by[30]

$$\mathbf{U}(x) = 2k_B T \ln \Phi(A, x) \tag{3}$$

where

$$\begin{aligned}\Phi(A, x) &= y_1(A, x) + \mathcal{B}y_2(A, x)\\ &= \exp\left(-\frac{k_S x^2}{4k_B T}\right)\left[{}_1F_1\left(\frac{A}{2}+\frac{1}{4}, \frac{1}{2}; \frac{k_S}{2k_B T}x^2\right)\right.\\ &\quad \left. + \mathcal{B}x\sqrt{\frac{k_S}{k_B T}}\,{}_1F_1\left(\frac{A}{2}+\frac{3}{4}, \frac{3}{2}; \frac{k_S}{2k_B T}x^2\right)\right]\end{aligned} \tag{4}$$

with $-1/2 \leq A < 0$ and $\mathcal{B} < \mathcal{B}_c = \sqrt{2}\frac{\Gamma(A/2+3/4)}{\Gamma(A/2+1/4)}$, where ${}_1F_1(\alpha, \beta; z)$ represents the confluent hypergeometric function[31,32] and k_S is the stiffness of the optical trap[8,33] or the curvature of the potential barrier. Different values of the real parameter A, $-1/2 \leq A < 0$ correspond to different heights of the bistable potential well. The biasing parameter $\mathcal{B}$ governs the degree of asymmetry in the double-well such that $\mathcal{B} < \mathcal{B}_c$, where $\mathcal{B} > 0$ indicates that the depth of the left potential well is greater than that of the right, and vice versa for $\mathcal{B} < 0$. However, for $\mathcal{B} = 0$, eq 4 represents a symmetric bistable potential well.

The determination of the TPT and Kramers's FPT for the conformational transition of the aptamer in viscoelastic cellular environments governed by the power-law correlated thermal fluctuations requires the evaluation of the conditional probability distribution function $P(x, t|x_0)$. Thus, the conditional probability of locating the reaction coordinate x of the riboswitch at time t in the asymmetric potential well, given that it was situated at x_0 at an initial time $t = 0$, is defined by $P(x, t|x_0)$. $P(x, t|x_0)$, which may be obtained as the solution of the effective FPE[5,22] in the asymmetric potential energy landscape defined by eq 3 as (refer to the Supporting Information of ref 5 for the details of the calculations)

$$\frac{\partial P(x, t|x_0)}{\partial t} = D(t)\left[\frac{\partial^2}{\partial x^2} + \frac{\partial}{\partial x}\frac{\mathbf{U}'(x)}{k_B T}\right]P(x, t|x_0) \tag{5}$$

where $D(t)$ is the time-dependent diffusion coefficient of the riboswitch aptamer in the viscoelastic cellular environment that may be expressed as

$$D(t) = \frac{k_B T}{k_S}\frac{\dot{\mathcal{Z}}(t)}{\mathcal{Z}(t)} \tag{6}$$

with

$$\mathcal{Z}(t) = E_{\beta,1}\left(D_\beta\frac{k_S}{k_B T}t^\beta\right) \tag{7}$$

where $E_{a,b}$ represents the two-parameter Mittag−Leffler function.[34] $D_\beta = (k_B T/\eta_\beta)$ nm^2 μs$^{-\beta}$ and for $\beta = 1$, $D_1 = (k_B T/\eta)$ nm^2 μs^{-1}; here, D_1 corresponds to the normal diffusion of the riboswitch in completely homogeneous surroundings, whereas D_β depicts the diffusion coefficient in heterogeneous cellular environments of varying viscoelasticities. These two different diffusion coefficients may be related as[5,22] $0 < D_\beta/D_1 \leq 1$ with the scaling exponent β, where $0 < \beta \leq 1$. This scaling exponent determines the degree of complexity/heterogeneity of the surrounding medium. Typical experimental values of these diffusion coefficients reported for the structural transitions of the aptamer in a normal diffusive environment are given by $D_1 = 0.2$ nm^2 μs^{-1} and $D_1 = 0.02$ nm^2 μs^{-1}, without and with ligand binding,[9] respectively.

Equation 5 is solved by the method of separation of variables through bilinear expansion in the spatial and the temporal domain, which may be simplified to yield[27]

$$\begin{aligned}P(x, t|x_0) &= C_0^2\sqrt{\frac{k_S}{k_B T}}\frac{1}{(\Phi(A, x))^2} + \sum_{n=0}^{\infty} C_{n+1}^2\sqrt{\frac{k_B T}{k_S}}\\ &\quad (\Phi(A, x_0))^2\frac{d}{dx}\frac{D_n(x)}{\Phi(A, x)}\frac{d}{dx_0}\frac{D_n(x_0)}{\Phi(A, x_0)}\mathcal{Z}(t)^{-(n+A+\frac{1}{2})}\end{aligned} \tag{8}$$

where $D_n(x)$ is the parabolic cylinder function,[31,35] defined as $D_n(x) = 2^{-n/2}\exp(-ax^2/2)H_n(x\sqrt{a})$, and $H_n(x)$ is the Hermite polynomial.[31,35] The normalization constants of the ground and excited states are denoted by $C_0^2 = \left(\frac{\mathcal{B}_c^2 - \mathcal{B}^2}{2\mathcal{B}_c}\right)$ and $C_{n+1}^2 = \frac{1}{\sqrt{2\pi}n!\left(n+A+\frac{1}{2}\right)}$; $n \geq 0$, respectively (refer to the Supporting Information of ref 5 for the details of the calculations).

https://doi.org/10.1021/acsphyschemau.1c00056
ACS Phys. Chem Au 2022, 2, 353−363

2.1. FPT Distribution and MFPT

FPT[36,37] is the time required by the riboswitch aptamer for the conformational transition from one potential well at one side of the free energy barrier to the other over the barrier for the first time. This time is also referred to as Kramers's FPT.[21,38,39] Appropriate boundary conditions are applied to evaluate the FPT statistics of the unfold and fold transitions of the riboswitch aptamer in an asymmetric bistable potential well.

The unfold and fold conformational transitions of the riboswitch aptamer may be viewed as a 1D diffusion across a free energy barrier as observed in the single-molecule experiments.[25,40,41] The minima of the potential well correspond to the fully folded state F and the P1 unfolded state P1_U of the riboswitch aptamer, where the well depths characterize the respective stability of the folded and P1 unfolded states. The transition events may be categorized as (i) F ↔ P1_U (without ligand binding) and (ii) F·L ↔ P1_U + L (i.e., with ligand binding), where the symbol ↔ denotes the reversible transitions between the folded and unfolded states. The two transitions via routes (i) and (ii) are considered as decoupled.

For both transitions (i) and (ii), the fully folded state, F, resides at a lower potential well which denotes a relatively more stable conformation as compared to the P1 unfolded state, P1_U. However, the presence of the ligand (adenine) further stabilizes the folded state F, and hence, F·L has a lower energy as compared to that of F. These states are modeled via absorbing boundary conditions since the aptamer undergoes a complete conformational transition from one state to the other. The FPT distribution (FPTD) for the conformational transitions of the riboswitch aptamer via route (i) and (ii) with and without ligand binding may be described via the conditional probability distribution function as

$$\mathcal{F}(x_0, t) = -\frac{\mathrm{d}}{\mathrm{d}t}\int_{x_A}^{x_B} P(x, t|x_0)\,\mathrm{d}x \tag{9}$$

where x_A and x_B define the initial and the final positions corresponding to the respective conformations for the unfold-fold transitions in the absence and presence of the ligand. For example, x_A and x_B may be recast as x_F and x_U for F → P1_U, whereas $x_{F\cdot L}$ and x_U denote the reaction coordinates for F·L → P1_U + L, respectively. The conformational transitions (i) and (ii) may be defined for any arbitrary reaction coordinate, x_0 in the region $x_A < x_0 < x_B$, where x_A and x_B denote the initial and final states for (i) and (ii), respectively. The FPTD, $\mathcal{F}(x_0, t)$ for the conformational transition in an asymmetric bistable potential in complex cellular environments for either transitions may be calculated as

$$\mathcal{F}(x_0, t) = \sum_{n=0}^{\infty} C_{n+1}^2 \sqrt{\frac{k_B T}{k_S}}\,(\Phi(A, x_0))^2 \frac{\mathrm{d}}{\mathrm{d}x_0}\frac{D_n(x_0)}{\Phi(A, x_0)} \left[\frac{D_n(x)}{\Phi(A, x)}\right]\Bigg|_{x_A}^{x_B} \left(D_\beta \frac{k_S}{k_B T} t^{\beta-1}\right)\left(n + A + \frac{1}{2}\right) E_{\beta,\beta}\left(D_\beta \frac{k_S}{k_B T} t^{\beta}\right)\left[E_{\beta,1}\left(D_\beta \frac{k_S}{k_B T} t^{\beta}\right)\right]^{-(n+A+\frac{3}{2})} \tag{10}$$

The MFPT,[27,42] $\overline{\tau}$, represented as $\overline{\tau} = \int_0^\infty t\mathcal{F}(x_0, t)\,\mathrm{d}t$, corresponds to the average time required for each transition, that is, either (i) or (ii) to recross and revisit its initial conformation until it reaches its final state. Therefore, the MFPT for the conformational transitions of the riboswitch aptamer with and without ligand binding under power-law correlated memory effects in cellular environments may be expressed as

$$\overline{\tau} = \sum_{n=0}^{\infty} C_{n+1}^2 \sqrt{\frac{k_B T}{k_S}}\,(\Phi(A, x_0))^2 \frac{\mathrm{d}}{\mathrm{d}x_0}\frac{D_n(x_0)}{\Phi(A, x_0)} \left[\frac{D_n(x)}{\Phi(A, x)}\right]\Bigg|_{x_A}^{x_B} \left(\frac{k_B T}{k_S D_\beta}\right)^{1/\beta}\left[\frac{2\Gamma(1+\beta)}{(2n + 2A + 1)}\right] \tag{11}$$

2.2. Survival Probability

The associated survival probability[37] $S_p(t)$, of the folded (unfolded) state of the *add* A-riboswitch aptamer to reside in its respective potential well before the transitions via routes (i) and (ii), may be mathematically characterized through the spatial integral of the conditional probability distribution $P(x, t|x_0)$ of the reaction coordinate and hence may be expressed as

$$S_p(t) = \int_{x_A}^{x_B} P(x, t|x_0)\,\mathrm{d}x \tag{12}$$

The generalized expression of the survival probability for the conformational transitions of the *add* A-riboswitch aptamer with and without the ligand in the heterogeneous environments is given by

$$S_p(t) = C_0^2 \left[\frac{x'^{1}F_1\left(\frac{A}{2} + \frac{3}{4}, \frac{3}{2}; \frac{x'^2}{2}\right)}{{}_1F_1\left(\frac{A}{2} + \frac{1}{4}, \frac{1}{2}; \frac{x'^2}{2}\right) + \mathcal{B}x'\,{}_1F_1\left(\frac{A}{2} + \frac{3}{4}, \frac{3}{2}; \frac{x'^2}{2}\right)}\right]\Bigg|_u^v + \sum_{n=0}^{\infty} C_{n+1}^2 \sqrt{\frac{k_B T}{k_S}}\,(\Phi(A, x_0))^2 \frac{\mathrm{d}}{\mathrm{d}x_0}\frac{D_n(x_0)}{\Phi(A, x_0)}\left[\frac{D_n(x)}{\Phi(A, x)}\right]\Bigg|_{x_A}^{x_B} \mathcal{Z}(t)^{-(n+A+\frac{1}{2})} \tag{13}$$

where $u = \sqrt{\frac{k_B T}{k_S}}\,x_A$ and $v = \sqrt{\frac{k_B T}{k_S}}\,x_B$.

2.3. TPT Distribution and MTPT

TPT[23,43] may be defined as the time required by the *add* A-riboswitch aptamer to just cross the potential barrier in its transit between one conformation located at one side of the parabolic potential barrier, x_A (or x_B), to the other situated across the barrier, x_B (or x_A), via the transition state, x_{TS}, at the barrier top, without revisiting its initial position. The TPT distributions (TPTDs) of unfold and fold transitions are obtained within the confined domain $x_{A1} < x_{TS} < x_{B1}$, with the appropriate absorbing boundaries at x_{A1} and x_{B1}, to prevent the revisit of each of the trajectories to their initial states. Thus, the TPTD, $\mathcal{P}_{TPT}(t)$ for the riboswitch aptamer in the bounded domain, across the inverted parabolic potential barrier for $A = -1/2$ and $\mathcal{B} = 0$, may be expressed as

$$U(x)|_{A=-1/2} = -\frac{k_S x^2}{2} \tag{14}$$

The TPTD, $\mathcal{P}_{TPT}(t)$ for the structural transitions of the riboswitch aptamer to dwell in between the $x_{A1} < x < x_{B1}$ region, for the parabolic potential defined by eq 14, is given as[18,27,37,43−45]

https://doi.org/10.1021/acsphyschemau.1c00056
ACS Phys. Chem Au 2022, 2, 353−363

$$\mathcal{P}_{\mathrm{TPT}}(t) = -\frac{\mathrm{d}}{\mathrm{d}t}\int_{x_{\mathrm{A}_1}}^{x_{\mathrm{B}_1}} P(x, t|x_0)|_{A=-1/2}\mathrm{d}x \tag{15}$$

MTPT,[21,23,46] $\overline{\tau}_{\mathrm{TPT}}$, is the average time required by the structural transitions of the riboswitch aptamer in a heterogeneous cellular environment between the two conformations across the parabolic potential barrier. This time that may be evaluated as

$$\overline{\tau}_{\mathrm{TPT}} = \sum_{n=1}^{\infty} \frac{2^{-n}}{\sqrt{\pi}} \frac{\Gamma(1+\beta)}{nn!}\left(\frac{k_{\mathrm{B}}T}{k_{\mathrm{S}}D_{\beta}}\right)^{1/\beta} \exp\left(-\frac{\Delta E}{k_{\mathrm{B}}T}\right) H_{n-1}\left(\sqrt{\frac{\Delta E}{k_{\mathrm{B}}T}}\right) H_n\left(\sqrt{\frac{k_{\mathrm{S}}}{2k_{\mathrm{B}}T}}\,x\right)\Bigg|_{x_{\mathrm{A}_1}}^{x_{\mathrm{B}_1}} \tag{16}$$

where

$$\frac{\Delta E}{k_{\mathrm{B}}T} = \frac{k_{\mathrm{S}}{x_0}^2}{2k_{\mathrm{B}}T} \tag{17}$$

Here, eq 17 portrays a linear relation between the potential barrier curvature and the dimensionless barrier height.[5,22,43]

3. SIMULATION DETAILS

An implicit SMD simulation is performed to analyze the first passage dynamics of the riboswitch. The template structure of the *add* adenine riboswitch aptamer is obtained from the RCSB (PDB ID: 1Y26) (refer to Figure 1a). The aptamer without the ligand is obtained by removing the adenine ligand manually from 1Y26. The SMD simulation of the riboswitch aptamer with and without the ligand is performed using AMBER *ff99bsc0* and *χOL3* force field[47,48] with NAMD-2.14 suite of programs.[49] Initially, all unfavorable interactions in the riboswitch aptamer are removed through energy minimization, followed by a two-step increase in temperature to 300 K. The system is equilibrated for 5 ns without using any periodic boundary constraints, followed by multiple production runs of 20 ns of the equilibrated aptamer. The temperature of the system is kept constant throughout all production runs via a Langevin thermostat.[50] The Born radius cutoff for each atom is fixed to 12.0 Å. To unfold the RNA, constant-force SMD simulations both with and without the ligand are performed by applying a constant force on the C5′ atom of the C1 residue while fixing the C3′ atom of the G71 residue of the aptamer. Since all conformational states of the aptamer are observed at 10 pN,[5,24] the SMD simulations are performed at this particular force to study the dynamics of the rate-limiting step[24] (i.e., F ↔ P1_U) both with and without the ligand.

SMD simulation snapshots of the unfolding events with and without adenine binding at 10 pN pulling force for the rate-limiting step are shown in Figure 2a,b, respectively. The end-to-end distance between C3′ and C5′ atoms (i.e., extension) of the folded state of the riboswitch aptamer is 16.52 Å. Initially, this distance is maintained in the SMD simulation as the folded state of the aptamer is stable, but with increasing simulation time, the P1 helix starts to unfold as the native contacts between nucleotides break due to the constant pulling force on the C5′ atom of the C1 residue of the aptamer. This constant pull completely unfolds the P1 helix, and the ligand unbinds itself from the aptamer during that time. This extension is a function of the simulation time, which is reported as 68.05 Å in the presence of the adenine ligand, while it is found to be 68.81 Å in the absence of the ligand that denotes the unfolding of the P1 helix of the riboswitch aptamer.

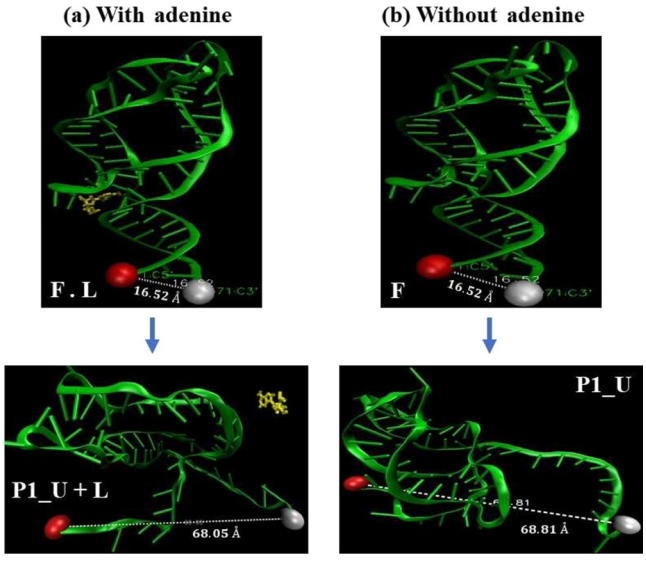

Figure 2. Snapshots of the riboswitch unfolding for the rate-limiting steps in the (a) presence and (b) absence of the ligand (adenine shown in yellow) obtained from the SMD simulations at 10 pN. The extensions between C3′ (gray) and C5′ (red) atoms of the P1_U state are (a) 68.05 (b) 68.81 Å in the presence and absence of the ligand, respectively.

4. RESULTS AND DISCUSSION

The conformational transitions of the *add* A-riboswitch aptamer between F and P1_U states across the asymmetric bistable potential represented by eq 3 are shown in Figure 3. Specific values of the parameters in eq 3 for the unfold and fold transitions of the P1 helix both with (blue) and without (black) ligand binding are chosen to match the results obtained from theory[5] with those of the experiments.[3] Experimentally estimated values of the free energy of unfolding of the P1 helix of the riboswitch aptamer in the ligand-unbound state is 10 ± 1 kcal/mol, while it is 18 ± 2 kcal/mol on binding with the ligand.[3] Figure 3 also presents an inverted parabolic potential (red) obtained from eq 3 for the definite values of $A = -1/2$ and $\mathcal{B} = 0$, which corresponds to the transition paths that describe the shortest trajectory between the folded and the unfolded states across the potential barrier.[5,18,43,44]

Figure 4 depicts the FPTD, $\mathcal{F}(t)$ of the conformational transition of the *add* A-riboswitch aptamer obtained from eq 10 plotted as a function of time. Figure 4a,b represents the unfold-fold transitions of the riboswitch aptamer without and with the ligand, respectively for three different values of β as $\beta = 0.8$ (blue), $\beta = 0.9$ (red), and $\beta = 1$ (black) with the respective values of the diffusion coefficients as D_β as $D_{0.8} = 0.16\ \mathrm{nm}^2/\mu\mathrm{s}^{0.8}$, $D_{0.9} = 0.18\ \mathrm{nm}^2/\mu\mathrm{s}^{0.9}$, and $D_1 = 0.2\ \mathrm{nm}^2/\mu\mathrm{s}$ for transitions without ligand binding and $D_{0.8} = 0.016\ \mathrm{nm}^2/\mu\mathrm{s}^{0.8}$, $D_{0.9} = 0.018\ \mathrm{nm}^2/\mu\mathrm{s}^{0.9}$, and $D_1 = 0.02\ \mathrm{nm}^2/\mu\mathrm{s}$ for transitions with ligand binding, respectively. The dashed and solid lines in Figure 4 denote the unfolding and folding of the P1 helix, respectively.

For each of these transitions, the FPTD is represented by an asymmetrically distributed unimodal peak. The amplitude of the peaks obtained for either transitions, with/without ligand,

https://doi.org/10.1021/acsphyschemau.1c00056
ACS Phys. Chem Au 2022, 2, 353−363

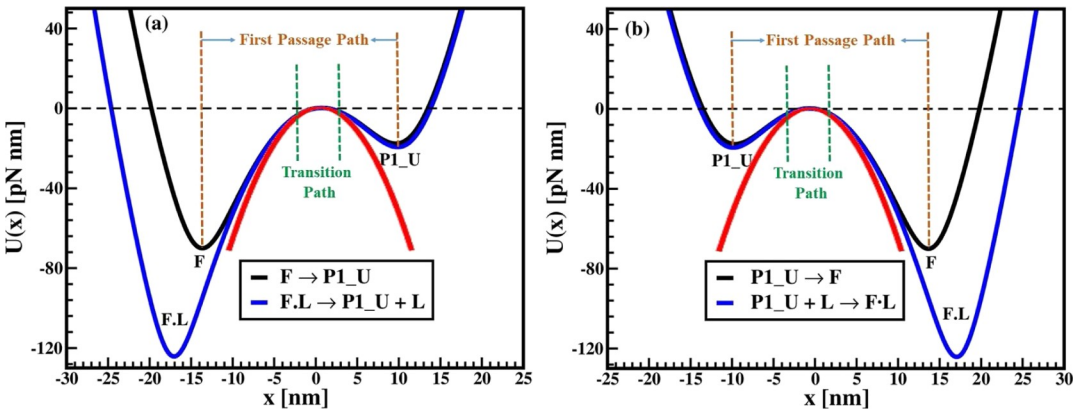

Figure 3. Asymmetric bistable potential, $\mathbf{U}(x)$ vs x, of the unfold (a) and fold (b) transitions of the riboswitch aptamer both with and without the ligand obtained from eq 3 as reconstructed for an experimentally determined potential.[3] Free energy landscape for the unfold and fold transitions in the absence of the ligand corresponds to 10 kcal/mol = 69.20 pN nm obtained for $A = -0.43$, $\mathcal{B} = 0.073$ and $A = -0.43$, $\mathcal{B} = -0.073$, respectively. Free energy in the presence of the ligand corresponds to 18 kcal/mol = 124.56 pN nm for $A = -0.44$, $\mathcal{B} = 0.0717$ and $A = -0.44$, $\mathcal{B} = -0.0717$, respectively.

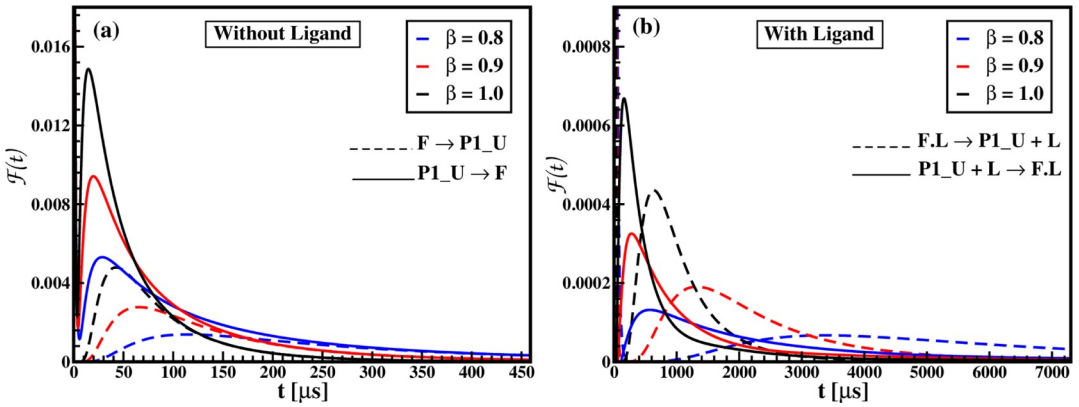

Figure 4. FPTD, $\mathcal{F}(t)$ vs time for the fold-unfold and unfold-fold transitions of the *add* A-riboswitch in the asymmetric potential well obtained from eq 10. Plots (a) and (b) depict the unfold and fold transitions of the aptamer without and with the ligand, respectively. The solid and dashed lines denote the fold and unfold transitions, respectively. Plots (a) and (b) are obtained using the following parameters: $D_{0.8} = 0.16$ nm$^2/\mu s^{0.8}$, $D_{0.9} = 0.18$ nm$^2/\mu s^{0.9}$, and $D_1 = 0.2$ nm$^2/\mu$s and $D_{0.8} = 0.016$ nm$^2/\mu s^{0.8}$, $D_{0.9} = 0.018$ nm$^2/\mu s^{0.9}$, and $D_1 = 0.02$ nm$^2/\mu$s.

decreases with the decrease in β values. The lower the value of β, the higher is the viscoelasticity (complexity) of the surroundings, which implies to increased correlations of the thermal fluctuations in a cellular environment.[22,29] Lower values of β correspond to a more complex viscoelastic environment which retards the motion of the riboswitch and hence reduces its FPTDs. The higher β values correspond to a more homogeneous environment, facilitating faster transitions of the aptamer among the unfolded and folded states with shorter FPTs.

A comparison of the FPTD of the *add* A-riboswitch transitions from the folded to the P1 unfolded state or vice-versa with and without ligand binding reveals that the FPTD for the fold-unfold transitions is much lower and broadly distributed as compared to that of the of unfold-fold transitions which are sharper and narrowly distributed for both (i) and (ii). The result implies less probable transitions of the riboswitch from the folded to the unfolded state, which exhibits a higher FPT as compared to the unfold-fold transitions.

Figure 5 represents a comparative plot of the FPTD profiles of these conformational transitions of the aptamer obtained from the SMD simulations at 10 pN and that of the theory calculated from eq 10 (for $\beta = 1$). Figure 5a,b depicts the FPTDs of the fold-unfold transitions, whereas Figure 5c,d shows the unfold-fold transition of the riboswitch both without and with ligand binding. Results of the theory are in good agreement with those of the SMD simulations for both transitions.

Figure 6 portrays the MFPT of the *add* A-riboswitch aptamer in an asymmetric bistable potential as a function of the reaction coordinate x_0 obtained from eq 11. Figure 6a,b presents the MFPT of the structural transitions of the riboswitch both in the absence and presence of the ligand, respectively, for three different values of β as $\beta = 0.8$, $\beta = 0.9$, and $\beta = 1$ which defines varying degrees of complexity in the cellular medium.

The results illustrate that the MFPT for transitions (i) and (ii) of the riboswitch aptamer monotonically increases with an increase of the viscoelasticity of the surrounding environment (i.e., a decrease in the β value) and subsequently assumes a constant value. This is due to the "caging" effect[5,22,23,44] imparted by the heterogeneous cellular environment which retards the structural motion of the riboswitch, thereby restricting its conformational transition. Thus, the MFPT of the riboswitch increases in heterogeneous surroundings as

https://doi.org/10.1021/acsphyschemau.1c00056
ACS Phys. Chem Au 2022, 2, 353−363

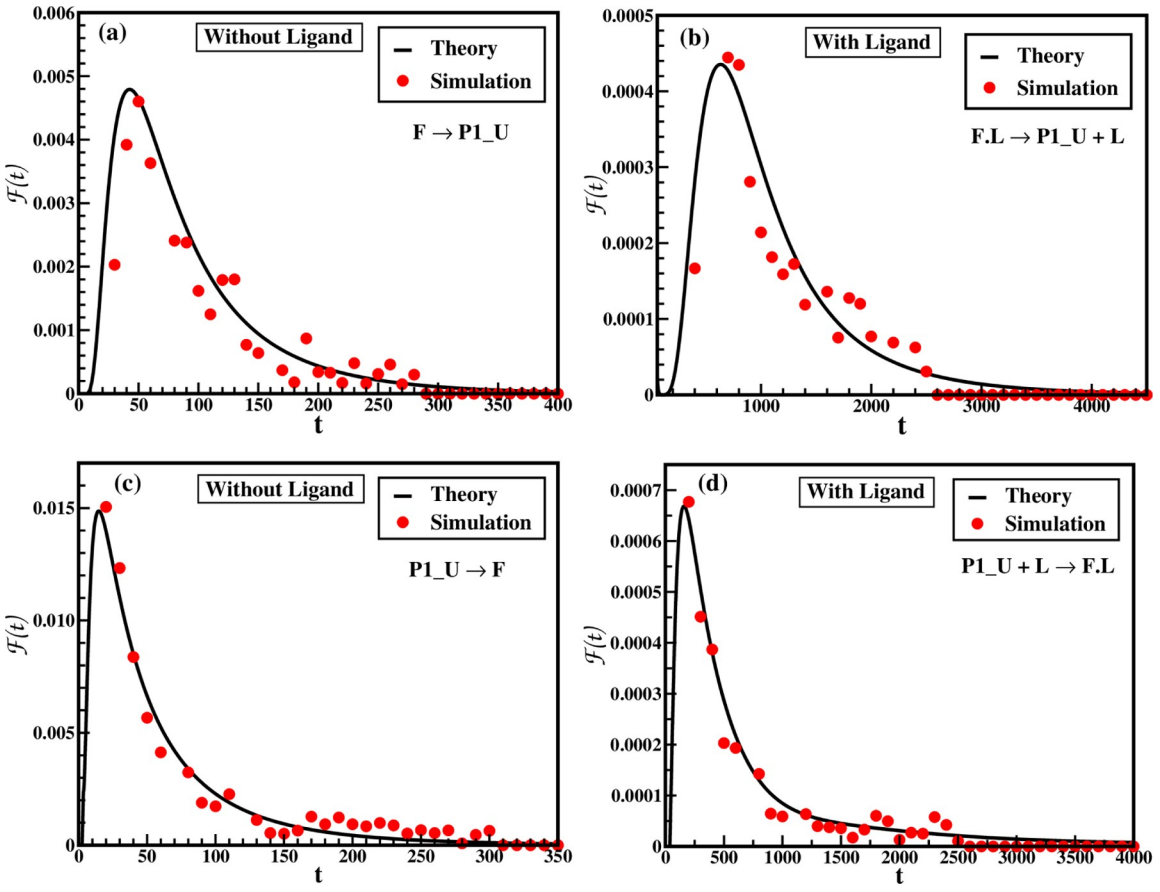

Figure 5. Comparison of the FPTD obtained from the SMD simulations (red circle) and those of theory (for $\beta = 1$, black line) for the structural transitions of the riboswitch aptamer (a,c) without and (b,d) with ligand binding for both fold-unfold and unfold-fold transitions.

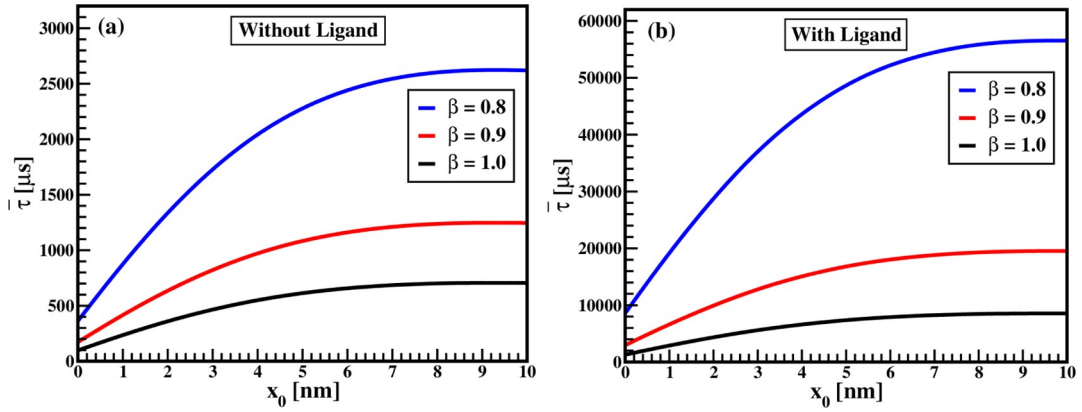

Figure 6. MFPT, $\bar{\tau}$ vs the extension (or the reaction coordinate) of the unfold-fold transition of the riboswitch aptamer as obtained from eq 11. Plots (a,b) predict the MFPT in the absence and presence of the ligand, respectively.

compared to that of the homogeneous one. A significant quantitative difference with higher MFPT is observed for the unfold-fold transition of the riboswitch aptamer for transition (ii) as compared to (i). Ligand binding in the triple helix junction of the *add* A-riboswitch stabilizes its structure due to an increase in the tertiary interactions between two hairpin loops. Hence, the ligand-bound state becomes more stable than its ligand-unbound state and requires a larger energy to reach the P1 unfolded state.

MFPT for unfold-fold transitions of the riboswitch aptamer obtained from the SMD simulations at 10 pN are compared with those of the theory calculated from eq 11 (for $\beta = 1$) in Figure 7. Results of the theory agree well with those of the SMD simulations both in the presence and absence of the ligand.

Figure 8 represents the survival probability of the unfold-fold transitions of the *add* A-riboswitch in the folded or the unfolded states for transitions (i) and (ii), respectively, for three different values of β as $\beta = 0.8$, $\beta = 0.9$, and $\beta = 1$. Figure 8a,b depicts the survival probability for transitions (i) and (ii) of the riboswitch aptamer both without and with ligand binding as a function of time. The results portrayed in Figure 8 are obtained by truncating the infinite series and retaining up

https://doi.org/10.1021/acsphyschemau.1c00056
ACS Phys. Chem Au 2022, 2, 353−363

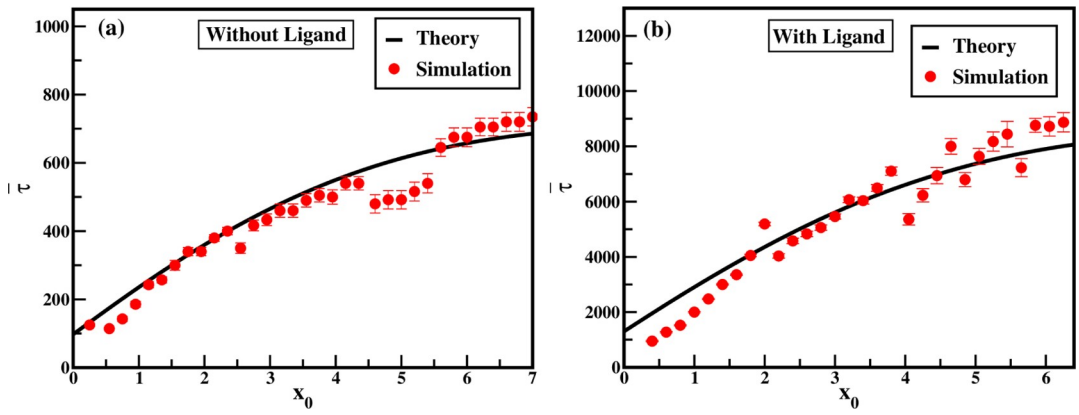

Figure 7. Comparison of the MFPT from SMD simulations (red circle) and theory (black line) for the ligand (a) unbound and (b) bound states of the riboswitch aptamer. The standard errors which are averaged over the mean time of crossing are shown by the error bars.

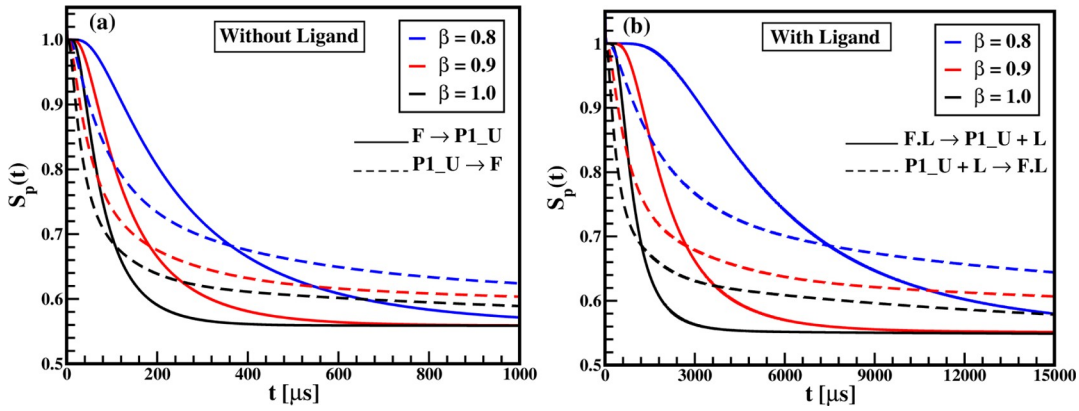

Figure 8. Survival probability, $S_p(t)$ vs time, calculated from eq 13 for different values of β. Plots (a,b) depict the unfold and fold transitions of the P1 helix of the *add* A-riboswitch aptamer without and with ligand binding, respectively. The solid and dashed lines represent the unfold and fold transitions of the riboswitch aptamer, respectively, both in the absence and presence of the ligand.

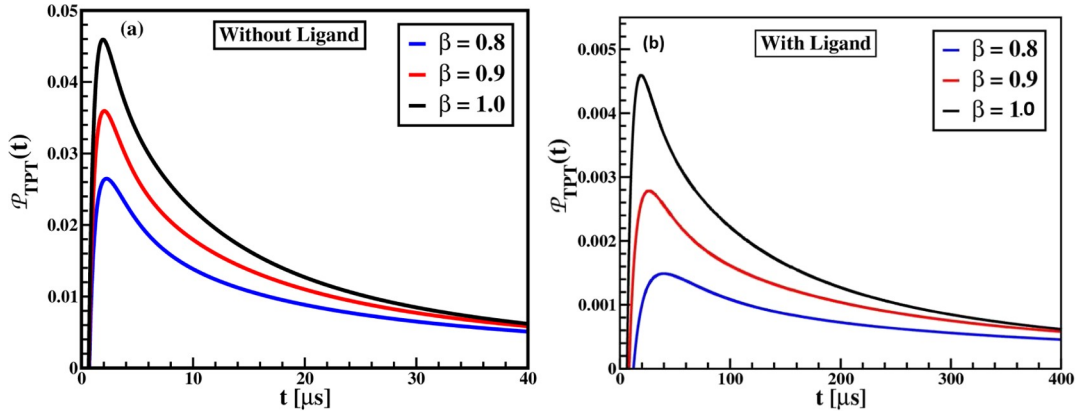

Figure 9. $\mathcal{P}_{TPT}(t)$ vs time t of the unfold-fold transitions of the riboswitch with ligand (a) unbound and (b) bound states across the potential barrier for different β values. $\mathcal{P}_{TPT}(t)$ calculated from eq 15 for β = 1.0 (black), β = 0.9 (red), and β = 0.8 (blue).

to 1000 terms as given in eq 13. This truncation is adequate enough to ensure precision.

The survival probability curves for transitions (i) and (ii) exhibit a stretched Mittag-Leffler decay unlike a simple exponential decay as observed in normal diffusion in completely homogeneous environments. The deviation from the normal diffusive behavior in viscoelastic cellular environments characterizes the anomalous diffusive dynamics of the riboswitch aptamer in an asymmetric free energy landscape. The rate of decay of the survival probability increases as it approaches a homogeneous environment. (i.e., with higher β values). The decay of the survival probability is much slower for both unfold-fold transitions in the presence of the ligand as compared to that in its absence. This is due to the fact that ligand binding stabilizes the structure of the riboswitch aptamer through tertiary interactions. The enhanced structural stability of the ligand-bound riboswitch aptamer makes the conformational transition less probable, which is reflected in a

https://doi.org/10.1021/acsphyschemau.1c00056
ACS Phys. Chem Au 2022, 2, 353−363

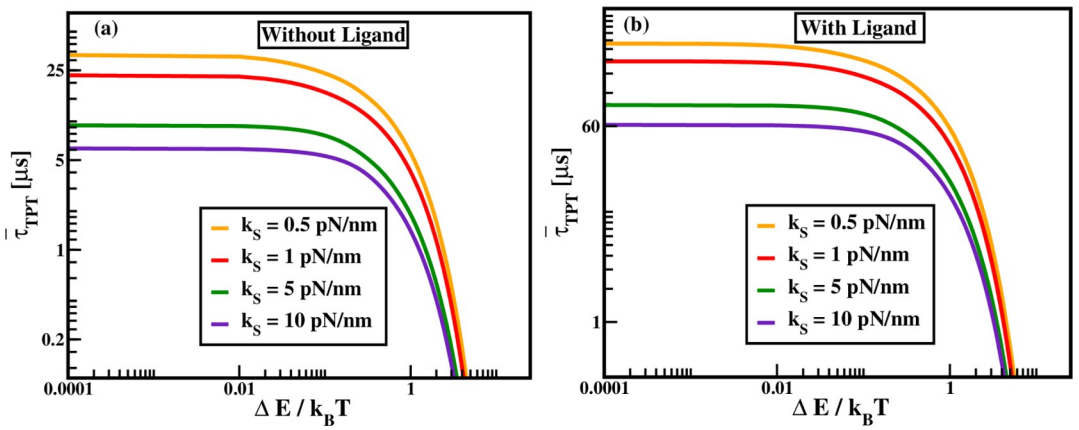

Figure 10. MTPT, $\bar{\tau}_{TPT}$ of the riboswitch aptamer as a function of the barrier height, $\Delta E/k_BT$ for k_S = 0.5 pN/nm, k_S = 1 pN/nm, k_S = 5 pN/nm, and k_S = 10 pN/nm with β = 1.

slower decay of the probability. The survival probability shows a faster decay for the folding transitions in the short-time regime, while the decay becomes sluggish in the long-time regime as compared to the unfolding transitions both with and without the ligand. This suggests that the P1 unfolded state has a higher propensity for the more-stable folded state; therefore, its probability to survive in the potential well decays faster as compared to that of the folded state at shorter times.

Figure 9 represents the TPTD, $\mathcal{P}_{TPT}(t)$ for the conformational transition of the riboswitch aptamer between two states across the potential barrier as a function of time, t. The amplitude of the TPTD peaks decreases with a decrease in the values of β. The lower the β value, the higher is the complexity, which retards the motion of the riboswitch aptamer, and consequently increases its TPT to cross the barrier. Since the ligand-bound state is more stable, the corresponding TPTs are relatively higher as compared to the unbound ones.[5]

A comparison of the results for FPT and TPTDs is displayed in Figures 4 and 9. The plot reveals that the TPTs observed for the unfold and fold transitions of the riboswitch aptamer are lower than the FPTs. Unlike FPTD, the TPTD estimates the time required by the riboswitch to just cross the potential barrier, irrespective of the details of the actual transition mechanism, i.e., whether the TPTD corresponds to transitions via fold to the unfold state or vice versa. Since the FPTD accounts for the time to cover the entire molecular trajectory from one well to the other, it governs the exact pathway of the unfold and fold transitions.

In Figure 10, the MTPT, $\bar{\tau}_{TPT}$ of the conformational transition of the *add* A-riboswitch aptamer without and with the ligand is plotted for different values of the curvature of the potential barrier, k_S as a function of barrier height, $\Delta E/k_BT$. The different values are k_S = 0.5 pN/nm, k_S = 1 pN/nm, k_S = 5 pN/nm, and k_S = 10 pN/nm. MTPT portrays a monotonic decay with an increase in the barrier height. The MTPT decreases with an increase in the curvature of the barrier,[16] k_S.

Results depict that the magnitude of the MTPT for the ligand-bound state is approximately 10 times higher than that for the ligand-unbound state. Since adenine binding stabilizes the triple helix junction of the aptamer domain, the ligand-bound aptamer takes a longer time to cross the potential barrier.[5] For higher barrier heights, there is a negligible difference between the TPTDs of the *add* A-riboswitch aptamer obtained for free and absorbing boundary conditions. Therefore, a comparison of the value of MTPT of the riboswitch aptamer obtained from our theory with those obtained from the single-molecule experiments[9] for higher barrier heights (i.e., for k_S = 10 pN/nm) is shown in Table 1. The values of the MTPT calculated from our theory are in good agreement with the results obtained from experiments.[9]

Table 1. MTPT of Unfold/Fold Transition of the Riboswitch Calculated from Our Theory Is Compared with That Obtained by Woodside et al.[9]

MFPT	theory (μs)	experiments[9] (μs)
without ligand	6.1	5
with ligand	60.94	60

5. CONCLUSIONS

This work theoretically investigates the unfold and fold transitions of the adenine riboswitch as a stochastic dynamics of the reaction coordinate of the aptamer in an asymmetric bistable potential well within the framework of GLE. Theoretical results are qualitatively compared with those obtained from the SMD simulations. The estimated Kramers's FPTD reveals that the transitions of the riboswitch from the unfolded to the folded state are more probable and faster than those of the folded to the unfolded one. A comparative study of the distributions of TPT and Kramers's FPT indicates that the TPTs are faster than Kramers's FPT. The TPTDs are insensitive to the details of the exact transition mechanism unlike Kramers's FPTD. Survival probability follows a stretched Mittag-Leffler decay for the unfold-fold transitions, where the probability of the aptamer in the ligand-bound state shows a much slower decay as compared to that in the ligand-unbound one. MFPT of the riboswitch aptamer with and without ligand binding increases with an increase in the complexity/heterogeneity of the surrounding environment. The results of Kramer's FPT and MFPT for both fold and unfold transition obtained from the theory are in good qualitative agreement with those of SMD simulations. The values of the MTPT estimated analytically quantitatively agrees with those obtained from SMFS experiments for higher barrier heights.

https://doi.org/10.1021/acsphyschemau.1c00056
ACS Phys. Chem Au 2022, 2, 353−363

AUTHOR INFORMATION

Corresponding Author

Parbati Biswas − *Department of Chemistry, University of Delhi, Delhi 110007, India;* orcid.org/0000-0001-7709-2263; Phone: +91-11-27666646; Email: pbiswas@chemistry.du.ac.in

Authors

Shivangi Sharma − *Department of Chemistry, University of Delhi, Delhi 110007, India*

Vishal Singh − *Department of Chemistry, University of Delhi, Delhi 110007, India;* Present Address: Delhi School of Public Health, Institute of Eminence (DSPH-IoE), University of Delhi, Delhi 110007, India

Complete contact information is available at: https://pubs.acs.org/10.1021/acsphyschemau.1c00056

Author Contributions

†S.S. and V.S. contributed equally to this work.

Notes

The authors declare no competing financial interest.

ACKNOWLEDGMENTS

The authors gratefully acknowledge FRP Grant-IoE (IoE/2021/12/FRP) for financial support and SCFBio (IIT, Delhi) for providing adequate supercomputing facility. S.S. acknowledges UGC, India (Grant Schs/SRF/139/F-193/2012-13) for providing financial assistance in the form of SRF.

REFERENCES

(1) Mandal, M.; Boese, B.; Barrick, J. E.; Winkler, W. C.; Breaker, R. R. Riboswitches control fundamental biochemical pathways in Bacillus subtilis and other bacteria. *Cell* **2003**, *113*, 577−586.

(2) Barrick, J. E.; Breaker, R. R. The distributions, mechanisms, and structures of metabolite-binding riboswitches. *Genome Biol.* **2007**, *8*, R239.

(3) Neupane, K.; Yu, H.; Foster, D. A. N.; Wang, F.; Woodside, M. T. Single-molecule force spectroscopy of the *add* adenine riboswitch relates folding to regulatory mechanism. *Nucleic Acids Res.* **2011**, *39*, 7677−7687.

(4) Kim, J. N.; Breaker, R. R. Purine sensing by riboswitches. *Biol. Cell.* **2008**, *100*, 1−11.

(5) Sharma, S.; Singh, V.; Biswas, P. Effect of ligand binding on riboswitch folding: Theory and simulations. *J. Chem. Phys.* **2021**, *154*, 185101.

(6) Serganov, A.; Nudler, E. A decade of riboswitches. *Cell* **2013**, *152*, 17−24.

(7) Breaker, R. R. Riboswitches and the RNA world. *Cold Spring Harbor Perspect. Biol.* **2012**, *4*, a003566.

(8) Neupane, K.; Foster, D. A. N.; Dee, D. R.; Yu, H.; Wang, F.; Woodside, M. T. Direct observation of transition paths during the folding of proteins and nucleic acids. *Science* **2016**, *352*, 239−242.

(9) Neupane, K.; Ritchie, D. B.; Yu, H.; Foster, D. A.; Wang, F.; Woodside, M. T. Transition path times for nucleic acid folding determined from energy-landscape analysis of single-molecule trajectories. *Phys. Rev. Lett.* **2012**, *109*, 068102.

(10) Ritchie, D. B.; Woodside, M. T. Probing the structural dynamics of proteins and nucleic acids with optical tweezers. *Curr. Opin. Struct. Biol.* **2015**, *34*, 43−51.

(11) Greenleaf, W. J.; Woodside, M. T.; Block, S. M. High-resolution, single-molecule measurements of biomolecular motion. *Annu. Rev. Biophys. Biomol. Struct.* **2007**, *36*, 171−190.

(12) Neuman, K. C.; Nagy, A. Single-molecule force spectroscopy: optical tweezers, magnetic tweezers and atomic force microscopy. *Nat. Methods* **2008**, *5*, 491.

(13) Heus, H. A.; Puchner, E. M.; van Vugt-Jonker, A. J.; Zimmermann, J. L.; Gaub, H. E. Atomic force microscope-based single-molecule force spectroscopy of RNA unfolding. *Anal. Biochem.* **2011**, *414*, 1−6.

(14) Haller, A.; Soulière, M. F.; Micura, R. The dynamic nature of RNA as key to understanding riboswitch mechanisms. *Acc. Chem. Res.* **2011**, *44*, 1339−1348.

(15) Soukup, J. K.; Soukup, G. A. Riboswitches exert genetic control through metabolite-induced conformational change. *Curr. Opin. Struct. Biol.* **2004**, *14*, 344−349.

(16) Singh, V.; Biswas, P. A generalized Langevin equation approach for barrier crossing dynamics in conformational transitions of proteins. *J. Stat. Mech.: Theory Exp.* **2021**, *2021*, 063502.

(17) Singh, V.; Biswas, P. Conformational transitions of amyloid-β: A Langevin and generalized Langevin dynamics simulation study. *ACS Omega* **2021**, *6*, 13611−13619.

(18) Satija, R.; Das, A.; Makarov, D. E. Transition path times reveal memory effects and anomalous diffusion in the dynamics of protein folding. *J. Chem. Phys.* **2017**, *147*, 152707.

(19) Peters, B. *Reaction Rate Theory and Rare Events*; Elsevier, 2017.

(20) Pérez-Espinosa, A.; Aguilar-Cornejo, M.; Dagdug, L. First-passage, transition path, and looping times in conical varying-width channels: Comparison of analytical and numerical results. *AIP Adv.* **2020**, *10*, 055201.

(21) Kim, W. K.; Netz, R. R. The mean shape of transition and first-passage paths. *J. Chem. Phys.* **2015**, *143*, 224108.

(22) Sharma, S.; Biswas, P. Conformational transitions of a DNA hairpin through transition path times. *J. Stat. Mech.: Theory Exp.* **2020**, 073411.

(23) Chaudhury, S.; Makarov, D. E. A harmonic transition state approximation for the duration of reactive events in complex molecular rearrangements. *J. Chem. Phys.* **2010**, *133*, 034118.

(24) Lin, J.-C.; Thirumalai, D. Relative stability of helices determines the folding landscape of adenine riboswitch aptamers. *J. Am. Chem. Soc.* **2008**, *130*, 14080−14081.

(25) Greenleaf, W. J.; Frieda, K. L.; Foster, D. A. N.; Woodside, M. T.; Block, S. M. Direct observation of hierarchical folding in single riboswitch aptamers. *Science* **2008**, *319*, 630−633.

(26) Kubo, R.; Toda, M.; Hashitsume, N. *Statistical Physics II: Nonequilibrium Statistical Mechanics*; Springer Series in Solid-State Sciences, Vol. *31*; Springer, 1985.

(27) Gardiner, C. W. *Handbook of Stochastic Methods*, 2nd ed.; Springer Series in Synergetics, Vol. *13*; Springer, 1985.

(28) Sharma, S.; Biswas, P. Hydration water dynamics around a protein surface: a first passage time approach. *J. Phys.: Condens. Matter* **2017**, *30*, 035101.

(29) Sharma, S.; Biswas, P. Unusual dynamics of hydration water around motor proteins with long-ranged hydrodynamic fluctuations. *Phys. A* **2019**, *534*, 122045.

(30) Hongler, M. O.; Zheng, W. M. Exact solution for the diffusion in bistable potentials. *J. Stat. Phys.* **1982**, *29*, 317−327.

(31) Abramowitz, M.; Stegun, I. A. *Handbook of Mathematical Functions with Formulas, Graphs, and Mathematical Tables*; National Bureau of Standards Applied Mathematics Series, Vol. *55*; Dover: New York, 1964.

(32) Buchholz, H. *The Confluent Hypergeometric Function: with Special Emphasis on its Applications*; Springer Tracts in Natural Philosophy, Vol. *15*; Springer, 1969.

(33) Manuel, A. P.; Lambert, J.; Woodside, M. T. Reconstructing folding energy landscapes from splitting probability analysis of single-molecule trajectories. *Proc. Natl. Acad. Sci. U.S.A.* **2015**, *112*, 7183−7188.

(34) Gorenflo, R.; Kilbas, A. *Mittag-Leffler Functions, Related Topics and Applications*; Springer, 2016.

(35) Gradshteyn, I. S.; Ryzhik, I. M. *Table of Integrals, Series, and Products*; Academic Press, 2014.

(36) Zwanzig, R. *Nonequilibrium Statistical Mechanics*; Oxford University Press, 2001.
(37) Redner, S. *A Guide to First-Passage Processes*; Cambridge University Press, 2001.
(38) Hänggi, P.; Talkner, P.; Borkovec, M. Reaction-rate theory: fifty years after Kramers. *Rev. Mod. Phys.* **1990**, *62*, 251.
(39) Laleman, M.; Carlon, E.; Orland, H. Transition path time distributions. *J. Chem. Phys.* **2017**, *147*, 214103.
(40) Warhaut, S.; Mertinkus, K. R.; Höllthaler, P.; Fürtig, B.; Heilemann, M.; Hengesbach, M.; Schwalbe, H. Ligand-modulated folding of the full-length adenine riboswitch probed by NMR and single-molecule FRET spectroscopy. *Nucleic Acids Res.* **2017**, *45*, 5512−5522.
(41) Savinov, A.; Perez, C. F.; Block, S. M. Single-molecule studies of riboswitch folding. *Biochim. Biophys. Acta, Gene Regul. Mech.* **2014**, *1839*, 1030−1045.
(42) van Hijkoop, V. J.; Dammers, A. J.; Malek, K.; Coppens, M. O. Water diffusion through a membrane protein channel: A first passage time approach. *J. Chem. Phys.* **2007**, *127*, 085101.
(43) Caraglio, M.; Put, S.; Carlon, E.; Vanderzande, C. The influence of absorbing boundary conditions on the transition path time statistics. *Phys. Chem. Chem. Phys.* **2018**, *20*, 25676−25682.
(44) Medina, E.; Satija, R.; Makarov, D. E. Transition path times in non-Markovian activated rate processes. *J. Phys. Chem. B* **2018**, *122*, 11400−11413.
(45) Zhang, B. W.; Jasnow, D.; Zuckerman, D. M. Transition-event durations in one-dimensional activated processes. *J. Chem. Phys.* **2007**, *126*, 074504.
(46) Berezhkovskii, A. M.; Dagdug, L.; Bezrukov, S. M. Mean direct-transit and looping times as functions of the potential shape. *J. Phys. Chem. B* **2017**, *121*, 5455−5460.
(47) Pérez, A.; Marchán, I.; Svozil, D.; Sponer, J.; Cheatham, T. E., III; Laughton, C. A.; Orozco, M. Refinement of the AMBER force field for nucleic acids: improving the description of α/γ conformers. *Biophys. J.* **2007**, *92*, 3817−3829.
(48) Zgarbová, M.; Otyepka, M.; Šponer, J.; Mládek, A.; Banáš, P.; Cheatham, T. E., III; Jurečka, P. Refinement of the Cornell et al. nucleic acids force field based on reference quantum chemical calculations of glycosidic torsion profiles. *J. Chem. Theory Comput.* **2011**, *7*, 2886−2902.
(49) Phillips, J. C.; Braun, R.; Wang, W.; Gumbart, J.; Tajkhorshid, E.; Villa, E.; Chipot, C.; Skeel, R. D.; Kalé, L.; Schulten, K. Scalable molecular dynamics with NAMD. *J. Comput. Chem.* **2005**, *26*, 1781−1802.
(50) Van Gunsteren, W. F.; Berendsen, H. J. C. A leap-frog algorithm for stochastic dynamics. *Mol. Simul.* **1988**, *1*, 173−185.

https://doi.org/10.1021/acsphyschemau.1c00056
ACS Phys. Chem Au 2022, 2, 353−363